THE ASTROPHYSICAL JOURNAL, 394:363–377, 1992 July 20

THE *GALILEO* AND *PIONEER VENUS* ULTRAVIOLET SPECTROMETER EXPERIMENTS: SOLAR LYMAN-α LATITUDE VARIATION AT SOLAR MAXIMUM FROM INTERPLANETARY LYMAN-α OBSERVATIONS

W. R. PRYOR, J. M. AJELLO,[1] C. A. BARTH, C. W. HORD, A. I. F. STEWART, K. E. SIMMONS, W. E. MCCLINTOCK, B. R. SANDEL,[2] AND D. E. SHEMANSKY[3]
Laboratory for Atmospheric and Space Physics, University of Colorado, Boulder, CO 80309
Received 1991 October 3; accepted 1992 January 29

ABSTRACT

The *Galileo* ultraviolet spectrometer and *Pioneer Venus Orbiter* ultraviolet spectrometer (PVOUVS) experiments performed nearly simultaneous observations of the interplanetary Lyman-α emissions (IP Lyman-α) at solar maximum in 1990. The *Galileo* ultraviolet spectrometer experiment consists of an ultraviolet spectrometer (UVS) and an extreme-ultraviolet spectrometer (EUVS) both of which began acquiring IP Lyman-α data late in 1989. The PVOUVS has been in operation since 1978. A comparison is made of the latitude variation of the IP Lyman-α signal in 1986 at solar minimum from *Pioneer Venus* (*PV*) and in 1990 at solar maximum from *Galileo*. The *Galileo* EUVS shows a large enhancement of the IP Lyman-α emission has occurred over the intervening 4 years near the solar equator. An IP Lyman-α model has been developed which considers the latitude variation of the solar Lyman-α flux. The model is based upon the fraction of the solar disk occupied by plage regions. Low-latitude plage regions are the source of the enhanced Lyman-α flux near the solar equator. The model fit to the data shows a 25% decrease of the full disk solar Lyman-α flux from solar equator to solar pole in 1990. At the extremes of the solar cycle the dominant causes of IP Lyman-α asymmetries have now been determined from UVS observations spanning the region ecliptic pole to equator. The latitudinal variations in the solar Lyman-α radiation field are the explanation at solar maximum and the solar wind field is the basis at solar minimum. A detailed study of the *Galileo* IP Lyman-α observations on day-of-year (DOY) 190, 193, 197, and 200 in 1990 reveals large daily variations occur in response to the 27 day solar variation. Analysis of these data shows a maximum variation of 20% can be expected in the IP Lyman-α upwind intensity over this 27 day period.

Subject headings: Sun: activity — Sun: UV radiation

1. INTRODUCTION

An ecliptic-bound spacecraft with an ultraviolet-sensing instrument is capable of monitoring average solar properties at high solar latitudes by measuring Lyman-α emissions from interplanetary hydrogen. Asymmetries in the IP Lyman-α radiation field measurements extending from ecliptic pole to equator can be used to infer departures from spherical symmetry of the solar wind and solar Lyman-α. These inferences depend upon a model for the interplanetary hydrogen density (Thomas 1978). At present this method is the only experimental technique for finding the latitudinal variations in solar wind. The latitudinal variation of the solar wind at solar minimum was determined from *Mariner 10* and PVOUVS IP Lyman-α observations (Ajello 1990; Lallement & Stewart 1990; Witt, Ajello, & Blum 1979, 1981). Near-simultaneous observations of IP Lyman-α in 1990 by *Galileo* and *Pioneer Venus* provide an opportunity to determine the latitude variation in solar Lyman-α flux at solar maximum.

The *Galileo* spacecraft was placed on a gravity assist trajectory to Jupiter in 1989. The spacecraft encountered Venus on 1990 February 8, and then Earth on 1990 December 9. During the 10 month journey from Venus to Earth, the *Galileo* EUVS generally made observations of the IP Lyman-α twice a week. Figure 1 shows a north ecliptic view of the *Galileo* trajectory for the first 2 years of the mission. At the same time the PVOUVS continued to acquire IP Lyman-α data about twice a week as it has since 1978.

This paper will concentrate on spacecraft activity in 1990 July (DOY 190, 193, 197, 200) for *Galileo* and (DOY 201) for *PV*. The spacecraft locations for this period and the fields of view for the *Galileo* EUVS and PVOUVS swept in one rotation of the spinning sections of the two spacecraft are indicated in Figure 1. The *Galileo* EUVS is on the spinning section of the orbiter and views perpendicular to the spin axis which is pointed near the Sun for this part of the trajectory. The PVOUVS is also on a spinning spacecraft with the spin axis directed at the south ecliptic pole. The boresight of the PVOUVS is slanted at 60° with respect to the spin axis and maintains a look direction at 30° S ecliptic latitude. The *Galileo* EUVS scans nearly 360° through both ecliptic poles while the PVOUVS acquires data at 30° S scanning from near the interstellar hydrogen upwind direction (7°.1 N, 250°.5 E in ecliptic coordinates) to sidewind to downwind. For the particular observations described above, the combined *PV* and *Galileo* data sets give complementary information on the latitudinal and longitudinal behavior of the solar radiation fields at solar maximum.

Previous work has shown that continuous spacecraft observations of IP Lyman-α can simultaneously monitor both the solar Lyman-α line center flux and the solar wind flux over the solar cycle or the 27 day solar rotation (Ajello et al. 1987;

[1] Jet Propulsion Laboratory, California Institute of Technology, Pasadena, CA 91109.
[2] Lunar and Planetary Laboratory, 901 Gould-Simpson Building, University of Arizona, Tucson, Arizona 85721.
[3] Aerospace Engineering Department, University of Southern California, Los Angeles, CA 90089.

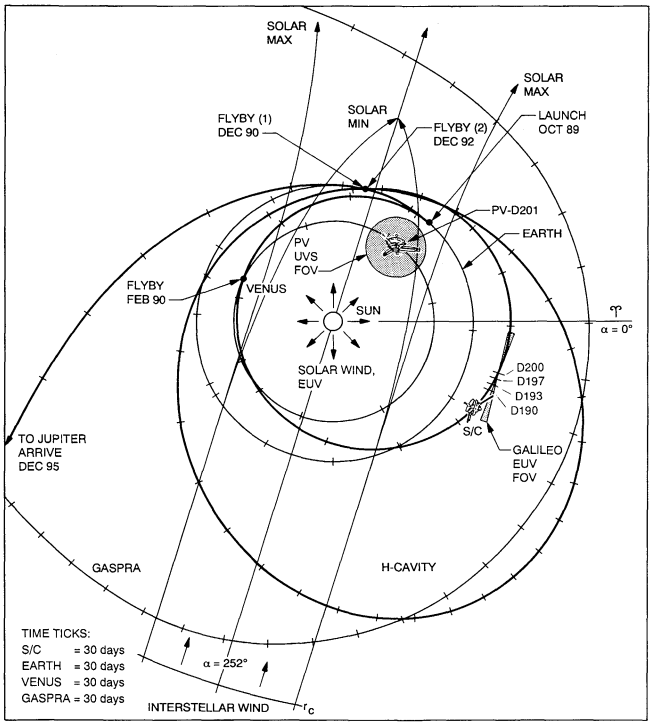

FIG. 1.—The *Galileo* and *Pioneer Venus* trajectories as seen from ecliptic north. The spacecraft locations at the time of the modeled observations are indicated. The PVOUVS field of view sweeps out a circle at 30° S denoted by shaded gray circle. The great circle through the ecliptic poles swept out by the *Galileo* EUVS is also indicated in shaded gray. The interstellar wind direction shows that the EUVS observed both the upwind and downwind directions during 1990 DOY 190–200 while the spacecraft was sidewind.

Ajello 1990). The *Galileo* EUVS measurements in 1990 are important since they occurred at the solar cycle maximum of solar cycle 22. The *Galileo* EUVS IP Lyman-α observations represent the first data set to be published describing the latitudinal variation of IP Lyman-α at solar maximum. *Voyagers 1* and *2* also have made cruise maneuver observations of the latitude variation of IP Lyman-α, since launch.

Previous analysis of data obtained at solar minimum from *Mariner 10* (Ajello 1978; Kumar & Broadfoot 1978; Ajello, Witt, & Blum 1979; Witt et al. 1979, 1981) and *Pioneer Venus* (Ajello et al. 1987; Ajello 1990) has shown that the solar wind flux is 18% less over the solar poles than over the solar equator. Observationally the effect of the latitude variation on IP Lyman-α sky background maps is to shift the upwind intensity maximum toward the north ecliptic pole. This paper will describe the latitudinal decrease of solar Lyman-α at solar maximum based on a model fit to the *Galileo* EUVS IP Lyman-α observations in 1990 July (DOY 190, 193, 197, 200). The results will be compared to a solar minimum model fit obtained for *PV* high-latitude data scans from 1986 and *Mariner 10* high-latitude data scans from 1974 to show that adequate models now exist to explain the entire solar cycle. The effect of this latitude variation at solar maximum is to cause a bulge in the sky background maps near the ecliptic equator.

The theory developed to model the solar Lyman-α latitudinal anisotropy is based upon the work of Cook, Brueckner, & VanHoosier (1980) and Cook et al. (1981). Their description of the latitudinal behavior of the full disk solar flux in terms of the fraction of the disk occupied by plages proved to be very useful at solar maximum. The model results for ecliptic plane viewing can be compared to Ca II K spectroheliogram images of the Sun provided by Sacramento Peak Observatory which show a concentration of plages at low latitudes. The fraction of the full disk occupied by plages is maximum for viewing in the ecliptic plane. For latitudes closer to the pole, the fraction of the disk occupied by plage regions is less. The longitudinal behavior of the full disk Lyman-α solar irradiance is derived from the combined solar proxy data sets of solar He I 1083 nm equivalent width measurements and the 10.7 cm radio flux (F10.7) cm radio flux. The helium data come from the Kitt Peak National Observatory and the F10.7 values come from the World Data Center of the National Oceanic and Atmospheric Administration.

2. INSTRUMENTATION AND IP LYMAN-α CRUISE DATA

The *Galileo* EUVS instrument has been described in detail previously (Hord et al. 1992). Initial results from the cruise operations have been reported in Hord et al. (1991). The EUVS instrument uses a mechanical collimator to restrict the instrumental field of view to 0°.87 by 0°.17, with the larger dimension parallel to the spacecraft spin axis. Light passes through the collimator and is focused and dispersed onto a 128 pixel bare microchannel plate detector by a holographically ruled concave grating in a Wadsworth configuration. The instrument covers the spectral range 55–125 nm with a resolution of 1.5 nm for point sources and 3.5 nm for extended sources. The EUVS instrument is mounted on the spinning section of the *Galileo* spacecraft. Data acquisition is initiated on each spin when the instrument boresight passes a point 45° before its closest approach to ecliptic north (if the commanded starting angle is 0°). The counts accumulated by the detector are read out every 21.3 ms until the commanded number of sectors of sky have been covered. For the observations discussed in this paper, the EUVS was commanded to have a starting angle of 1°.41, and 35 sky sectors each consisting of 25 detector readouts. For the reported spin rate of 3.149 rpm, each of the 35 sky sectors covered an area of 10°.1 by 0°.87, forming a nearly complete great circle directed almost pole-to-pole. The instrument has two data acquisition modes, cruise mode and encounter mode. The data described here were obtained in cruise mode, in which each reported count is added to the appropriate wavelength and sky sector bin in a data matrix in the instrument memory. A total of 21 detector pixels of a possible 128 were recorded at selected wavelengths in order to monitor interplanetary Lyman-α and He (58.4 nm) as well as the instrumental and stellar backgrounds. During cruise mode, the contents of the instrument memory are read out to the ground at irregular intervals, typically two to three times a week. The time resolution of cruise mode data is set by the frequency of memory readouts.

The *Galileo* UVS instrument (Hord et al. 1992) and PVOUVS instruments (Stewart 1980) are similar in design. They consist of Cassegrain telescopes that send light into Ebert-Fastie spectrometers with programmable plane gratings. Both instruments use Princeton EMR G photomultiplier tubes with a cesium iodide photocathode to monitor Lyman-α. The *Galileo* UVS Lyman-α observations cover a field of view of 1°.4 by 0°.1. During the *Venus* to *Earth* cruise period, the spacecraft scan platform moved the UVS on 12 occasions to obtain Lyman-α data in each of three directions: ecliptic north, the interstellar wind upwind direction, and a direction tangent to

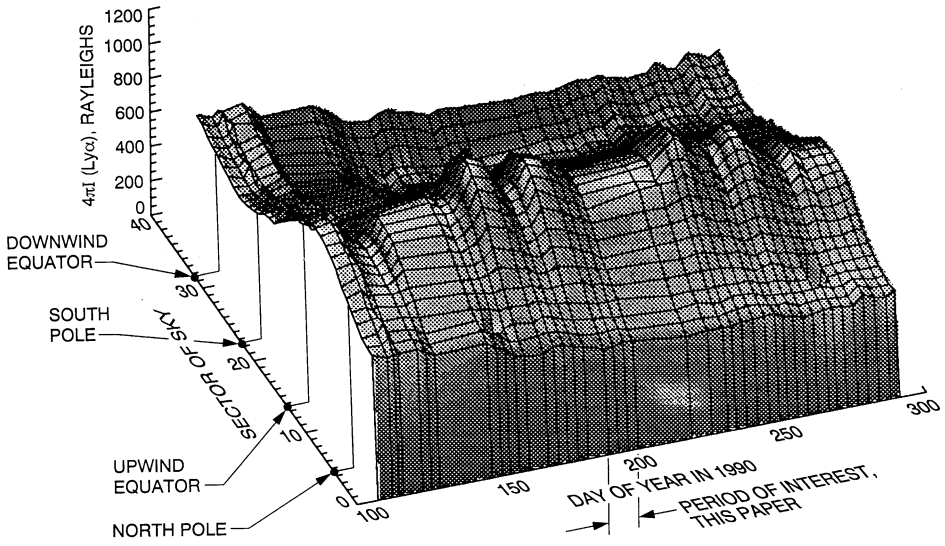

FIG. 2.—The IP Lyman-α brightness as a function of sky sector and DOY in 1990. Twenty-seven day waves in the intensity are visible where the sampling frequency was high. The period modeled in this paper is indicated.

the orbit of Earth near the time *Galileo* first crossed Earth orbit. Each direction was observed for 2 minutes. A full *Galileo* UVS spectrum consists of 528 grating positions, with a G-channel step size of 0.15 nm and a spectral resolution of 0.7 nm. For these Lyman-α observations, the grating was moved back and forth across the Lyman-α line in a 16 step "miniscan" covering both Lyman-α and the neighboring background wavelengths. The PVOUVS spins with the spacecraft and views in a direction 60° away from the spacecraft spin axis, typically in a circle at ecliptic latitude 30° S. The PVOUVS has a field of view of 1°.4 by 0°.14. It obtained Lyman-α data with the grating position set to a fixed position near line center.

Figure 2 presents an overview of the *Galileo* EUVS IP Lyman-α data obtained in the period from DOY 100–300 in 1990. The vertical axis measures the Lyman-α brightness in rayleighs. One horizontal axis represents the different sky sectors, while the other horizontal axis shows the time of a particular observation. The plot shows the sky is brightest in sectors near the upwind direction and dimmest in sectors close to the downwind direction. The data display strong temporal brightness variations. During several time intervals, the sampling frequency was sufficient to show these variations have a roughly 27 day period, which is correlated with the synodic rotation period of active regions on the Sun. Figure 3 presents EUVS data from selected sectors in Figure 2. The temporal variations in brightness in the two polar directions are much smaller than the variations seen in the sector closest to the ecliptic plane. This suggests the importance of including both longitudinal and latitudinal variations in the solar Lyman-α flux. *Galileo* UVS observations of Lyman-α in the ecliptic north direction made during the same time period are also shown and show good agreement with the EUVS ecliptic north measurements.

EUVS data from memory readouts on DOY 190, 193, 197, and 200 were selected for further study. These readouts represent the total counts obtained during each of four roughly 3 day periods. They were chosen because the spacecraft spin axis was not moved during this period (SCITURNS, an acronym for science turns, periodically shift the *Galileo* spin axis to keep it pointing near the Sun). Since the same great circle was observed throughout this period, variations in sky brightness can be attributed primarily to the Sun's 27 day rotation. Figure 4 shows the mean brightness derived for each time interval.

Pioneer Venus measurements provide an important check on the *Galileo* results, including instrumental calibrations (which affect the interplanetary hydrogen density determinations) and on other modeling parameters because of the different spacecraft location and viewing geometry. During 1986 the *PV* spin axis was turned to monitor Halley's comet. Observations were made in a circle extending from ecliptic latitudes 70° S to 50° N, similar to the geometry of *Galileo*, but near solar minimum. *Mariner 10* made Lyman-α observations

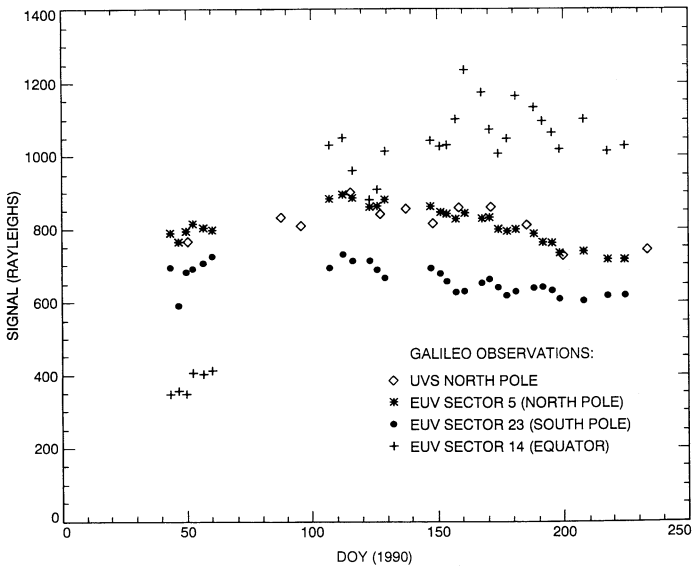

FIG. 3.—Lyman-α brightness measurements obtained by *Galileo* UVS viewing ecliptic north and three sky sectors of *Galileo* EUVS data from Fig. 2. One EUVS sky sector viewed ecliptic north, one viewed ecliptic south, and the third viewed directions lying near the ecliptic plane.

TABLE 1

TABLE OF SPACECRAFT GEOMETRY[a]

Spacecraft	Year	Date	DOY	X (AU)	Y (AU)	Z (AU)	R (AU)	λ (longitude)	σ/N
Galileo	1990	Jul 9	190	1.10	−0.52	−0.07	1.22	334°.7	1.0%
	1990	Jul 12	193	1.13	−0.48	−0.07	1.23	337.0	1.0
	1990	Jul 16	197	1.15	−0.44	−0.07	1.24	339.1	1.0
	1990	Jul 19	200	1.18	−0.40	−0.07	1.24	341.3	1.0
Pioneer Venus	1990	Jul 20	201	0.46	0.56	−0.02	0.75	50.6	2.7
	1986	Mar 4	63	0.72	0.095	−0.04	0.73	7.5	1.0
Mariner 10	1974	Jan 28	28	−0.50	0.56	0.03	0.73	131.8	9.0

[a] In ecliptic coordinates.

with a similar geometry to the *Galileo* EUVS near solar minimum in 1974. *PV* observations obtained on DOY 201 of 1990, close in time to the selected *Galileo* EUVS observations, were also chosen for modeling. The DOY 201 observations represent 1 hr of data obtained while the PVOUVS observed a circle near ecliptic latitude 30° S. Table 1 describes the data sets selected for modeling purposes. The data statistic σ/N, the standard deviation σ divided by the number of counts N obtained in that sampling bin, determines the complexity of the model required to fit the data.

3. SOLAR LYMAN-α FLUX DATA

The solar Lyman-α proxy model for the solar flux full disk irradiance for days 175–202 in 1990 is shown in Table 2. The solar Lyman-α flux is estimated from ground-based measurements of F10.7 and He I 1083 nm solar observations (Barth et al. 1990; Rottman & Barth 1990; Tobiska & Barth 1990). The daily variations in the solar flux are used to tabulate ecliptic g-values at 1 AU for Earth assuming that the solar Lyman-α integrated flux (photons cm^{-2} s^{-1}) and solar line center Lyman-α flux (photons cm^{-2} s^{-1} $Å^{-1}$) are numerically equal (Ajello et al. 1987). The g-value is the number of photons scattered per second per atom. The longitudinal behavior of the solar g-values at 1 AU for the longitude of the spacecraft is calculated assuming the Sun rotates 13°.3 per day as seen from Earth and the solar activity does not change for the 27 day period. The equatorial solar fluxes and g-values for days 175–202 in Table 2 are used for the analysis of the EUVS data readout from the *Galileo* spacecraft on day 190. Because these observations were made over the preceding 4-day period, the g-values that are appropriate for this analysis are the 27 day period centered on day 188. This same procedure was used for the data readouts from the spacecraft on days 193, 197, and 200. During the period from day 186 to day 200, the solar flux in the upwind direction (near 252° ecliptic longitude) decreased monotonically with time. This is reflected in the *Galileo* obser-

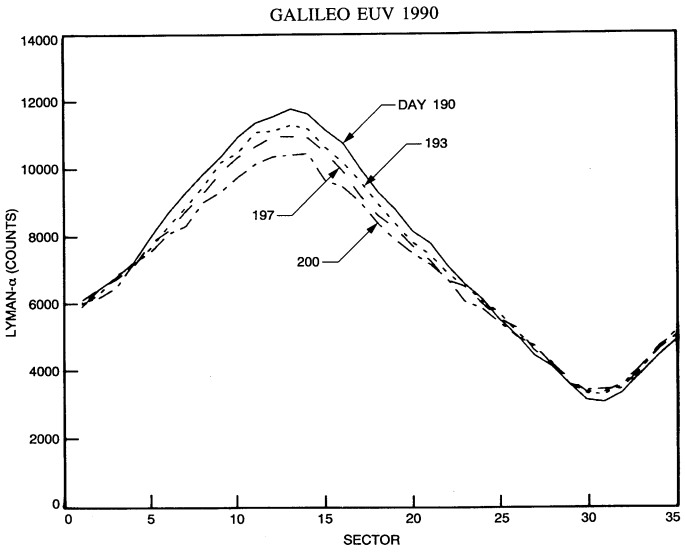

FIG. 4.—*Galileo* EUVS IP Lyman-α counts obtained from memory readouts on DOY 190, 193, 197, and 200 of 1990. The signal levels were normalized to a standard observation period of 80 hr. The actual observation periods differed from the standard period by 17% high, 15% low, 10% high, and 11% low for DOY 190, 193, 197, and 200, respectively.

TABLE 2

ECLIPTIC SOLAR FLUX VERSUS ECLIPTIC LONGITUDE ON DOY 188 IN 1990

1990 DOY of Measurement of Lyα Proxy	Solar Lyα Flux (10^{11} photons cm^{-2} s^{-1})	Lyα g-Value (10^{-3} photons s^{-1} $atom^{-1}$)	Longitude
175	3.48	1.89	98°.1
176	3.46	1.88	84.8
177	3.48	1.89	71.4
178	3.57	1.94	58.1
179	3.63	1.97	44.8
180	3.74	2.04	31.4
181	3.83	2.08	18.1
182	3.93	2.14	4.8
183	4.04	2.20	351.4
184	4.00	2.17	338.1
185	3.99	2.17	324.8
186	3.99	2.17	311.4
187	3.96	2.16	298.1
188	3.95	2.15	284.8
189	3.85	2.10	271.4
190	3.78	2.05	258.1
191	3.71	2.02	244.8
192	3.69	2.01	231.4
193	3.66	1.99	218.1
194	3.65	1.98	204.8
195	3.61	1.96	191.4
196	3.53	1.92	178.1
197	3.50	1.90	164.8
198	3.50	1.90	151.4
199	3.47	1.89	138.1
200	3.45	1.88	124.8
201	3.47	1.89	111.4
202	3.51	1.91	98.1

vations of the interplanetary Lyman-α in Figure 4 where the emission rate in the upwind direction decreases from day 190 to day 200.

Ca II K spectroheliograms are also used to understand the Lyman-α emission from the Sun. An extensive discussion of Ca II K emissions at 393.4 nm has been given by Lean (1987). The central core of the Ca II K emission is formed in the chromosphere as is the solar Lyman-α emission. The daily ground-based Ca II K spectroheliograms show the area of plage regions as do similar spectroheliograms in Lyman-α taken from space. Solar active regions have greater UV output than quiet regions. For Lyman-α, the contrast factor, C, defined as the ratio of active to quiet Sun intensity, is 4.6 (Cook et al. 1980, 1981).

For the period of observations considered in this paper for *Galileo*, *PV*, and *Mariner 10*, we have obtained the Ca II K spectroheliograms shown in Figure 5. There is a measurable area of plage regions only for the 1990 *Galileo* observations. The chromospheric networks of the third component of the Lean & Skumanich model (1983) are also seen in Figure 5*b*. Notice how the active regions near solar maximum occur predominantly at low solar latitudes in two longitudinal belts, one in each hemisphere. The effective area of plage regions in Lyman-α spectroheliograms obtained in space are larger than Ca II K features (Lean & Skumanich 1983).

4. SOLAR WIND LIFETIME OF H ATOMS

The density of hydrogen atoms near the Sun depends on the loss rate. The total lifetime of a hydrogen atom due to solar wind charge exchange and solar photoionization is given by

$$[\tau(\beta)]^{-1} = [\tau_{sw}(\beta)]^{-1} + [\tau_R(\beta)]^{-1}, \quad (1)$$

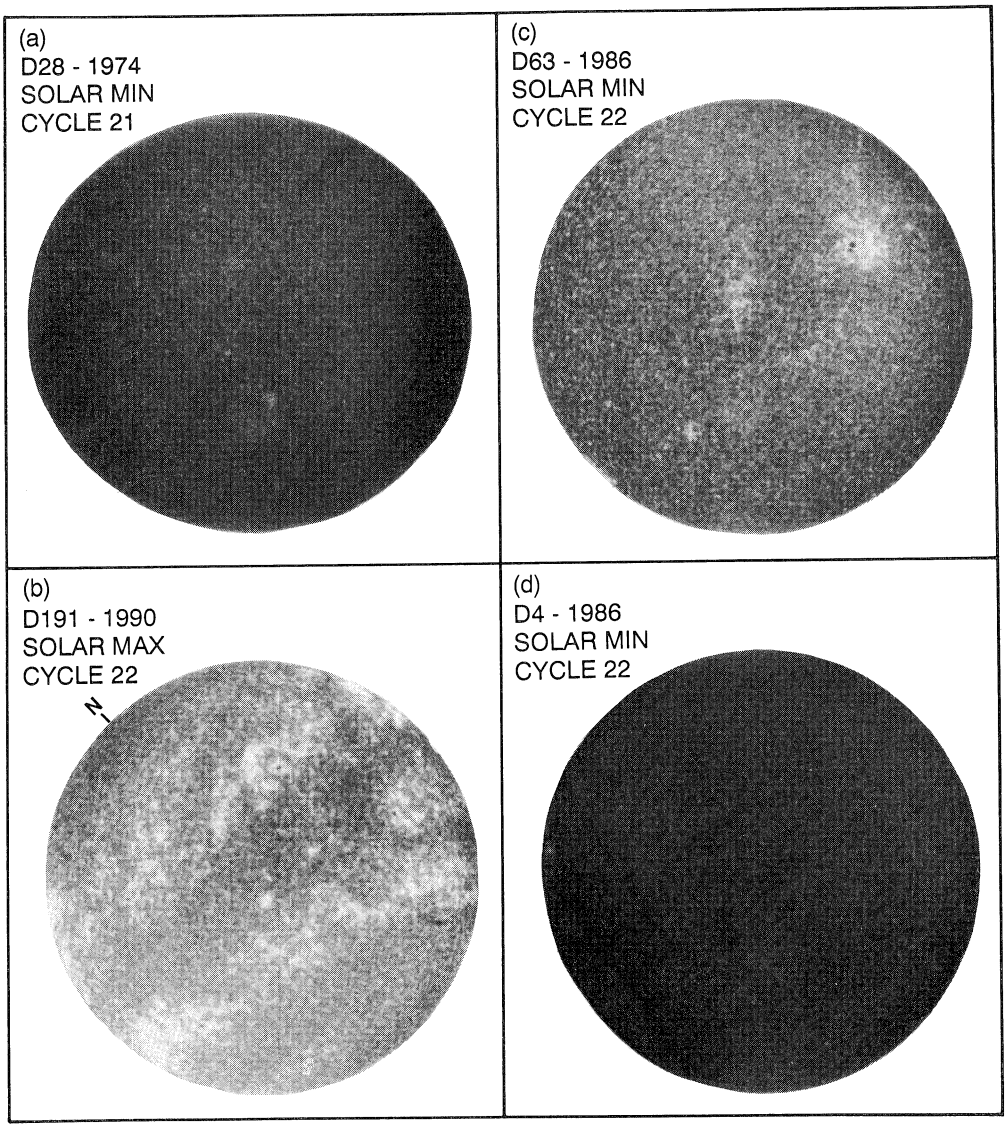

FIG. 5.—Ca II K images of the Sun (courtesy of Sacramento Peak Observatory), which indicate where Lyman-α excess emission from active regions will occur. The days chosen correspond to available Ca II K images closest in date to observations discussed in this paper. DOY 4 in 1986 was discussed in Ajello (1990). Note the difference between solar minimum and solar maximum plage areas. The north pole of the sun is indicated in (*b*).

TABLE 3

ECLIPTIC VALUE OF SOLAR WIND LIFETIME FROM *IMP 8* DATA IN 1990

Month	Average Solar Wind Flux (10^8 cm^{-2} s^{-1})	Average Solar Wind Velocity (km s^{-1})	Ecliptic H Lifetime[a] (10^6 s)
Jan	4.21	478	1.46
Feb	3.35	508	1.83
Mar	4.92	431	1.24
Apr	4.35	462	1.41
May	4.35	451	1.41

[a] Lifetime for charge-exchange only.

where τ is the total lifetime of the hydrogen atom at 1 AU; τ_{sw} is the solar wind charge exchange lifetime at 1 AU; τ_R is the photoionization lifetime of a hydrogen atom at 1 AU; and β is the solar latitude. We will show that τ_R can be assumed to be independent of latitude to within 6% for all phases of the solar cycle for a hydrogen atom. However, for a helium atom, the latitude dependence of photoionization lifetime is very important at solar maximum. We will describe this in a future paper. Values for the hydrogen atom photoionization lifetimes are given by Ajello et al. (1987) for various stages in the solar cycle. The value of τ_R used in this work at solar maximum is $\tau_R = 8.33 \times 10^6$ s.

The solar wind charge exchange lifetime for atomic hydrogen in the ecliptic plane can be determined by using the *IMP 8* data (A. Lazarus 1990, private communication) for 1990 together with the charge exchange cross section (Ajello et al. 1987). The average solar wind flux for each of the first 5 months of 1990 is given in Table 3. Table 3 also lists the solar wind lifetime due to charge exchange. The grand average of the solar wind lifetime due to charge exchange for the first 5 months of 1990 is 1.47×10^6 s compared to 1.81×10^6 s for the previous solar maximum (Ajello et al. 1987).

The solar wind lifetime due to charge exchange is also determined by comparison of the IP Lyman-α data with model predictions. These results will be discussed in the next section. The most recent models developed in Ajello (1990) show that the lifetime near solar minimum depends on solar latitude. The solar wind anisotropy is described in the model by a single parameter A. The parameter is assigned to the charge exchange lifetime by the relationship

$$[\tau_{sw}(\beta)]^{-1} = [1 - A \sin^2(\beta)]/\tau_0 , \quad (2)$$

where τ_0 is the equatorial charge exchange lifetime at 1 AU. Analysis of the *PV* and *Mariner 10* data at solar minimum shows that the rate of charge exchange with solar wind protons is 30% less over the solar poles than in the ecliptic, ($A = 0.3$). The A-value has not previously been determined at solar maximum. We initially assumed the A-value was the same (0.3) at both solar maximum and solar minimum. However, the required A-value at solar maximum to model the *Galileo* EUVS observations without a Lyman-α latitudinal anisotropy was found to be $A = -0.9$, which is not physically realistic. The pattern of Helmut streamers (Mihalov et al. 1990) outlining the magnetic field pattern of the Sun at solar maximum favors a more uniform solar wind flux than is found at solar minimum (A. J. Hundhausen 1990, private communication), i.e., $A \sim 0$. The models used will be considered in the next section. The *Galileo* IP Lyman-α analysis shows that the predominant latitudinal effect at solar maximum is the solar Lyman-α variation and that the best fit to the data is with $A \sim 0$.

5. SOLAR MAXIMUM MODEL

We have developed a model for analysis of IP Lyman-α observations based on the solar minimum data set of *PV* and *Mariner 10*. This IP Lyman-α backscatter model includes (1) solar wind asymmetries, (2) velocity distribution of H atoms, and (3) multiple scattering corrections. The model is described in Ajello et al. (1987) and Ajello (1990). The geometry for the backscatter calculation is shown in Figure 6. The boresights of

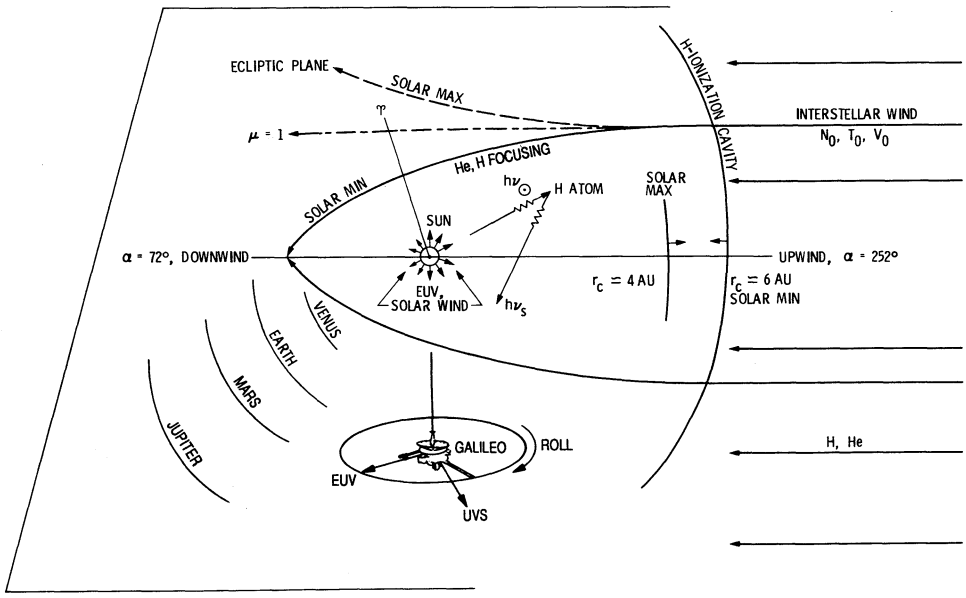

FIG. 6.—The geometry of the interstellar wind (ISW) atomic hydrogen backscatter problem. ISW atomic hydrogen approaching the Sun from the upwind direction is ionized by the solar wind, creating a cavity. The size of the cavity, r_c, depends on the solar wind flux. When μ, the ratio of radiation pressure to gravity, is one, the atoms are undeflected by the Sun. *Galileo* observes IP Lyman-α photons $h\nu_s$ scattered from the remaining neutrals.

the *Galileo* UVS and EUVS are indicated. The interstellar wind (ISW) parameters for number density, velocity, and temperature outside the solar system are denoted by N_0, V, and T, respectively. An initial attempt to apply the solar minimum model with $A = 0.3$ to the complete set of *Galileo*, *PV*, and *Mariner 10* IP Lyman-α data is shown in Figure 7. The *PV* data were previously modeled by Ajello (1990), while the *Mariner 10* data were modeled by Ajello (1978) and Witt et al. (1979). These data are presented here to show the dramatic change in the ecliptic latitude variation of IP Lyman-α from 1986 to 1990. All three data sets extend from the ecliptic equator to high ecliptic latitudes. Roll position is proportional to spin angle during a spin of the *Mariner 10* or *PV* spacecraft. Similarly for *Galileo* the EUVS sector denotes one of the 10°.1 sectors spanned in the sky during the spacecraft roll from ecliptic pole to equator and back again. This model fits the solar minimum observations of *Mariner 10* and *PV* but is inadequate for *Galileo*. The *Galileo* EUVS IP Lyman-α intensity is too bright at the equator. A negative, rather than positive, value of A is required to model the data. A positive value implies a signal enhancement at the poles as observed by *PV* in 1986 and *Mariner 10* in 1973–1974. For a positive value, the penetration of hydrogen atoms at the pole is enhanced due to the decrease of lifetime with latitude. The best fit to the *Galileo* data with the solar minimum model required an A-value of $A = -0.9$ and is shown in Figure 8.

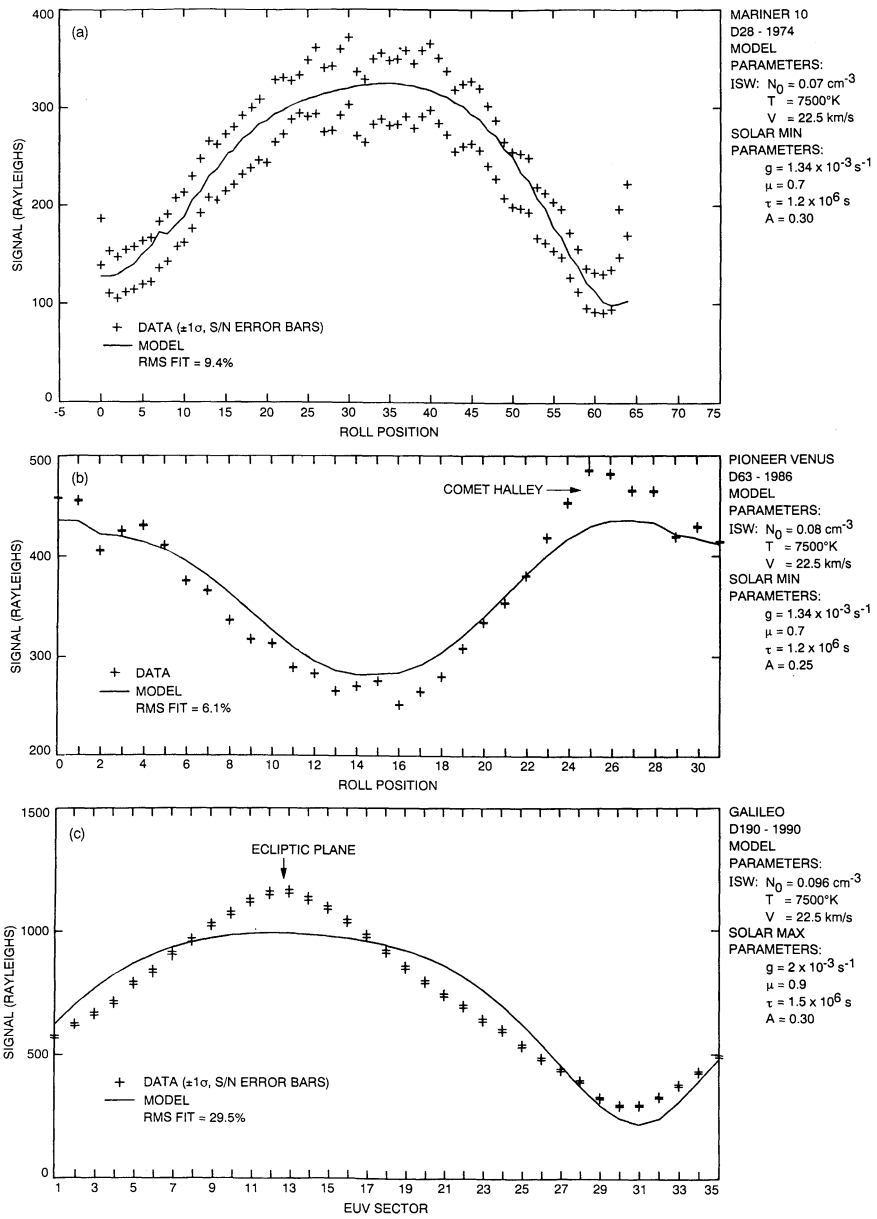

FIG. 7.—(*a*) The solar minimum model applied to polar great circle observations made by *Mariner 10* in 1974. This is roll 3 of Fig. 2 in Ajello (1978). The ISW parameters listed are the neutral hydrogen density N_0, temperature T, and velocity V outside of the solar system. The solar parameters are the Lyman-α resonance scattering coefficient g, μ, the hydrogen atom lifetime at 1 AU τ, and the solar wind asymmetry factor A. (*b*) The solar minimum model applied to high ecliptic latitude observations made by *Pioneer Venus* in 1986. The geometry for the observation is shown in Ajello (1990). The extra signal near roll position 24 is comet Halley. (*c*) An attempt to apply the solar minimum model to *Galileo* data from 1990 with $A = 0.3$, showing the relative brightness distribution has changed from 1986 to 1990.

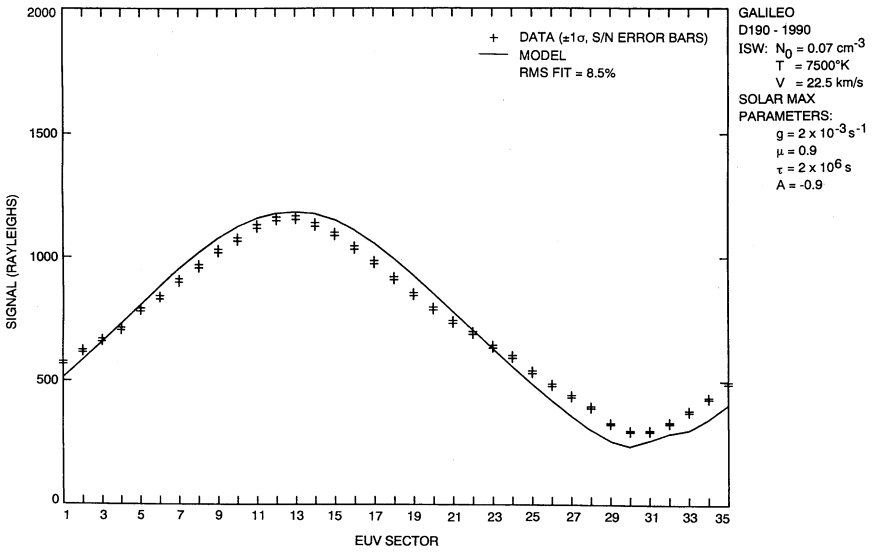

FIG. 8.—The best-fitting solar minimum model of the *Galileo* EUVS 1990 DOY 190 IP Lyman-α data. The solar minimum model can be forced to fit the data, but the derived value of $A = -0.9$ is unrealistic.

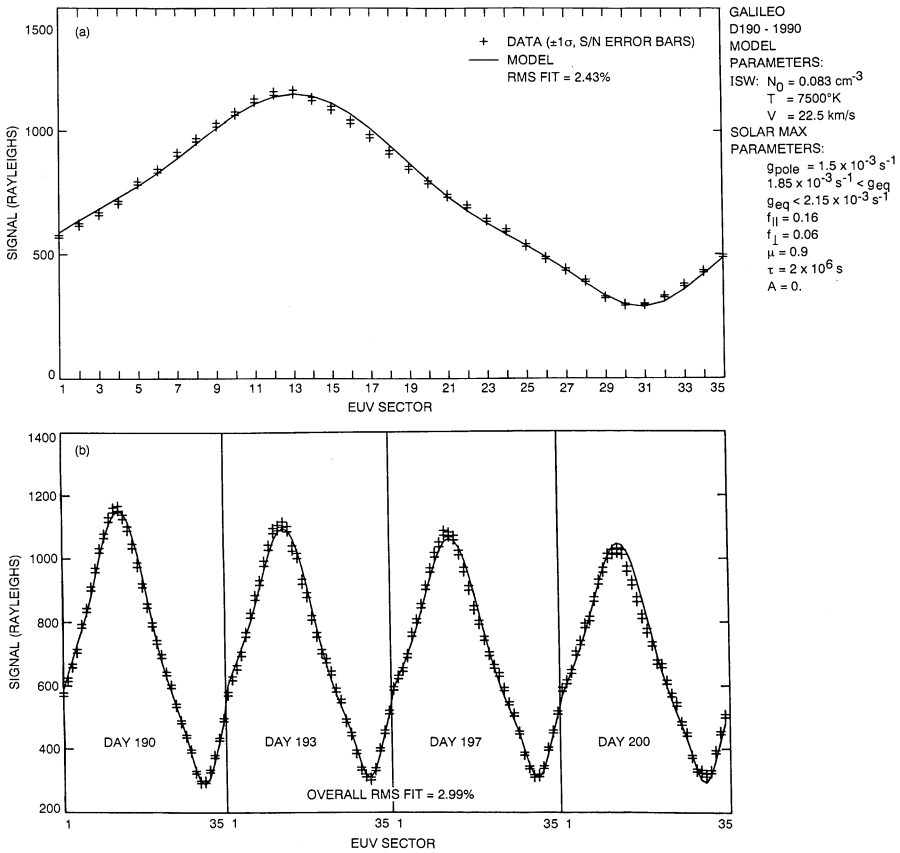

FIG. 9.—(*a*) The *Galileo* EUV IP Lyman-α data for 1990 DOY 190 compared to the new solar maximum model. The new solar parameters are g_{pole} and g_{eq}, the polar and equatorial Lyman-α resonance scattering coefficients, and $f_{\perp}$ and $f_{||}$, the polar and mean equatorial fractions of the Sun's projected disk covered by plage regions. (*b*) The *Galileo* EUVS Lyman-α data for DOY 190, 193, 197, and 200 compared to the same model. The figure indicates the modeling parameters for the ISW and the Sun. The RMS fit of the model to the data is given.

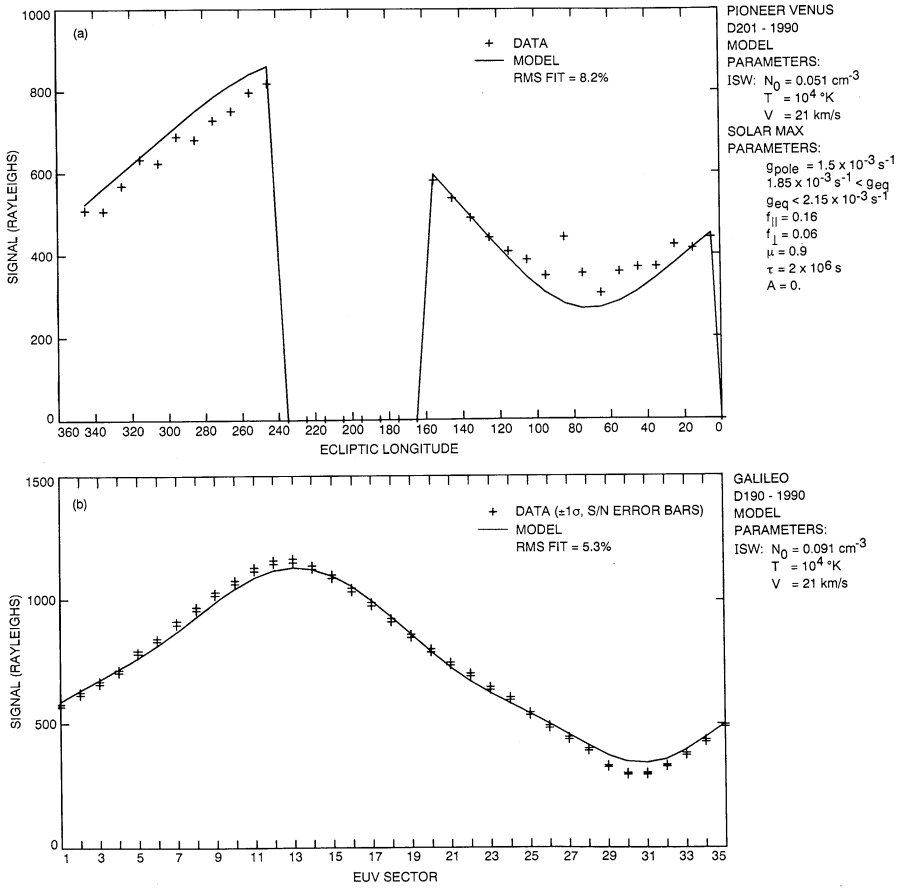

FIG. 10.—(*a*) The solar maximum model applied to PV 1990 DOY 201 Lyman-α data viewing near ecliptic latitude 30° S. Missing longitudes represent the planet Venus in the field of view. Stars are present in the data near ecliptic longitude 80°. (*b*) The same solar maximum model parameters applied to *Galileo* EUVS data from 1990 DOY 190.

With this result it became apparent that the solar minimum model did not contain the dominant solar effects controlling the IP Lyman-α intensity distribution. A more general model was needed. The Cook et al. model was employed which allows the *g*-value to vary with latitude. The important equations describing this model require a relationship using the directly measured equatorial solar *g*-value data from Table 2, and the *g*-value at the pole, a new modeling parameter: g_{pole} is the parameter that controls the amount of latitude variation between the equator and pole.

In this model, the *g*-value at any latitude, β, and longitude, λ, may be expanded in terms of a spherically symmetric quiet Sun value, g_{quiet}, and an active Sun with a position-dependent *g*-value. The subsolar *g*-value for any angular position in space is given by

$$g(\lambda, \beta) = g_{quiet} + g_{quiet}(C - 1)f(\lambda, \beta) . \quad (3)$$

The *g*-value is proportional to the full disk solar flux irradiance given by Cook et al. (1980, 1981). The first term in equation (3), g_{quiet}, is independent of latitude and has a value of 1.25×10^{-3} s^{-1} (Thomas & Anderson 1976). For the two-component model at solar maximum, $g(\lambda, \beta)$ is a mix of active network and quiescent Sun irradiance that occurs at solar minimum. The second term is the latitudinally and longitudinally dependent part of the *g*-value term, containing the low-latitude excess emission from both plage regions and active networks of contrast *C*. Plage and active network regions actually have slightly different contrast factors (Lean 1987). The fraction of flat disk filled with plages observed at any point in space at angular position (λ, β), $f(\lambda, \beta)$, is given by

$$f(\lambda, \beta) = f_{\perp} + [f_{||}(\lambda) - f_{\perp}] \cos^2(\beta) . \quad (4)$$

Here, $f_{||}$ refers to the fraction of the Sun's projected disk covered by plage regions seen from the Sun's equatorial plane, while $f_{\perp}$ is the fraction of the projected disk covered by plage regions when viewing from above the solar pole. Plages are nominally confined to a zone between 5° and 35° heliocentric latitude (Sheeley 1967). In the modeling procedure, $f_{\perp}$ is given by

$$f_{\perp} = (g_{pole} - g_{quiet})/[(C - 1)g_{quiet}] \quad (5)$$

and

$$f_{||}(\lambda) = (g_{eq}(\lambda) - g_{quiet})/[(C - 1)g_{quiet}] \quad (6)$$

in terms of $g_{eq}(\lambda)$ and g_{pole}, the *g*-values at $\beta = 0°$ and 90°, respectively. The free parameter in this model is g_{pole}, which has a best-fit value of 1.5×10^{-3} s^{-1}. The model uses the 7° offset of the solar rotation axis from the ecliptic pole to find $g_{eq}(\lambda)$, the *g*-value for longitude λ at a distance 1 AU above the solar equator, from the solar proxy model derived from measurements in the ecliptic plane at Earth.

6. MODEL RESULTS

The model results for the *Galileo* data are shown in Figure 9. Note the degree to which the structure in the model matches

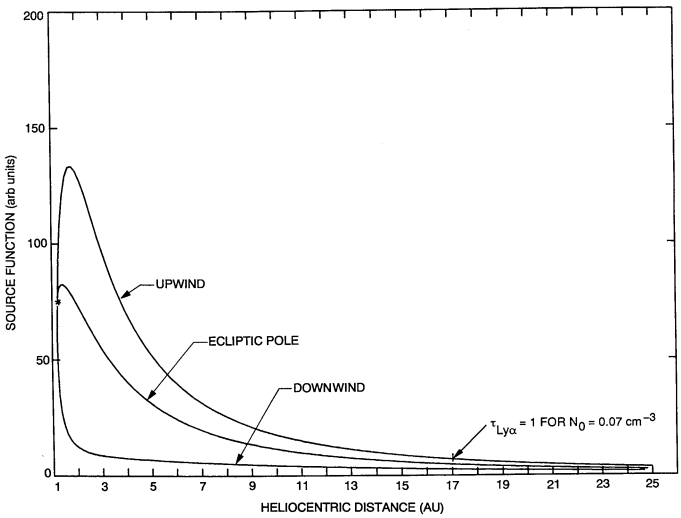

FIG. 11.—The source function for the Lyman emission emission as a function of heliocentric distance as seen from the *Galileo* spacecraft on DOY 190 of 1990 in the upwind, downwind, and ecliptic north directions. The spacecraft location and the source function value at the spacecraft are marked with an asterisk. $\tau_{Ly\alpha}$ is indicated, where $\tau_{Ly\alpha}$ is the IP Lyman-α line center optical depth measured from the spacecraft.

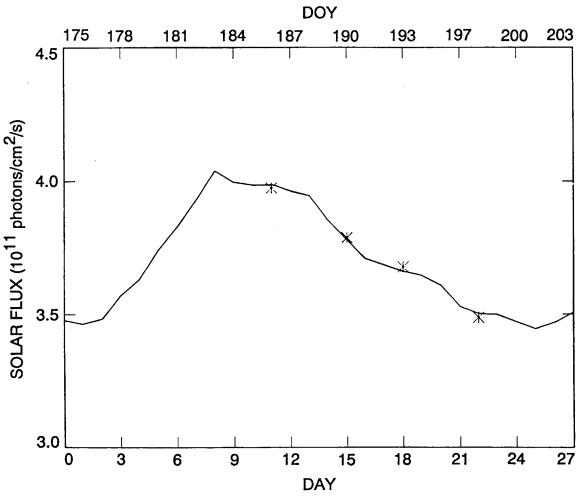

FIG. 13.—Modeled solar Lyman-α flux for day 175–202. Four data points marked with an asterisk are the result of a regression analysis of the interplanetary Lyman-α emission observed on days 188, 192, 196, and 199. This analysis indicates that the maximum in the Lyman-α source function is in the direction of ecliptic longitude 303°.

the data. Figure 9*a* shows the best fit for DOY 190. Figure 9*b* displays the same fits for the entire 4 day EUVS data set. The model matches the day-to-day decrease of the data in the upwind intensity described in the previous section. The improvement in the RMS fit from the solar minimum model of *PV* or *Mariner 10* is possible only because of the remarkable data quality and the development of a more general model with one additional free interstellar wind parameter, g_{pole}. An important goal of the modeling process is to develop a procedure to the point where it matches the data quality. The RMS difference for DOY 190 is 2.4%. The RMS difference for the four periods of interest is 3.0%. The data quality, given in Table 1, is only slightly better than the fit uncertainty. The modeling procedure indicates that the dominant solar effects on the ISW are now well understood.

While the *Galileo* EUVS was scanning the IP Lyman-α in ecliptic latitude, the PVOUVS was surveying the IP Lyman-α emissions in ecliptic longitude at 30° S latitude. We show in Figure 10 a simultaneous best fit to both data sets (*Galileo* DOY 190 and *PV* DOY 201) taking proper account of the solar rotation. The variation in three parameters (N_0, T, and V) arises from fitting both sets of data at the same time. We have accommodated the calibration difference between the two

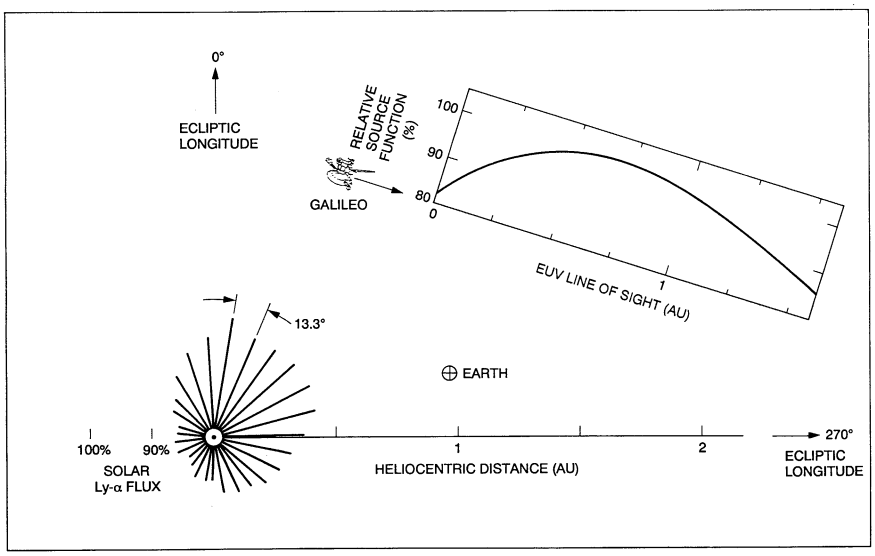

FIG. 12.—Location of the *Galileo* spacecraft, Earth, and the Sun in the ecliptic plane on DOY 188 of 1990. Earth is at ecliptic longitude 285°, and *Galileo* is at ecliptic longitude 334° and a heliocentric distance of 1.2 AU. The line of sight of the *Galileo* instrument is in the direction of ecliptic longitude 252°. The source function of the Lyman-α emission is plotted along the line of sight. The emission is normalized to 100% at the maximum, and only values between 80% and 100% are plotted. The 27 bars emanating from the Sun indicate the solar Lyman-α flux measured during the period DOY 175–202 of 1990. The flux is normalized to 100% at the maximum, and only values between 80% and 100% are plotted.

instruments by varying N_0, treating it as a normalization parameter to match the signal intensities. There is a calibration difference of nearly a factor of 2 between the two UVS instruments at Lyman-α. The dual fit is not as good as a model for each spacecraft data set considered separately. Based on the modeling results of the combined data set, the solar maximum model adequately explains the glow of IP Lyman-α from the entire celestial sphere to better than 10% uncertainty.

7. SOURCE FUNCTION

The best-fit model was used to calculate the source function (volume emission rate) for the interplanetary Lyman-α emission. In Figure 11, the source function as seen by the *Galileo* spacecraft is plotted as a function of heliocentric distance. The source function in the upwind direction (ecliptic longitude = 250°) is the largest and reaches a maximum at a heliocentric distance of 1.8 AU. The source function in the direction of the downwind cavity (ecliptic longitude = 70°) drops off immediately and does not reach a maximum. The viewing geometry of the *Galileo* spacecraft on day 190 in the ecliptic plane is shown in Figure 12. Earth was at an ecliptic longitude of 285°, and the *Galileo* spacecraft was at an ecliptic longitude of 334° and a heliocentric distance of 1.22 AU. The *Galileo* line of sight was in the direction, ecliptic longitude 252°. A portion of the source function is plotted in the figure along the *Galileo* line of sight. The data are normalized at the maximum, and only the values greater than 80% are plotted. Figure 12 also shows a broad maximum in the source function at a heliocentric distance of 1.8 AU and ecliptic longitude 303°.

As a test of the location of the maximum in the source function, the following analysis was performed. The values of the modeled solar Lyman-α flux centered at day 188 are plotted in Figure 13. These values are normalized to the maximum at day 183. A regression analysis was performed with this set of solar Lyman-α fluxes and the observed interplanetary Lyman-α emissions on days 188, 193, 197, and 199.

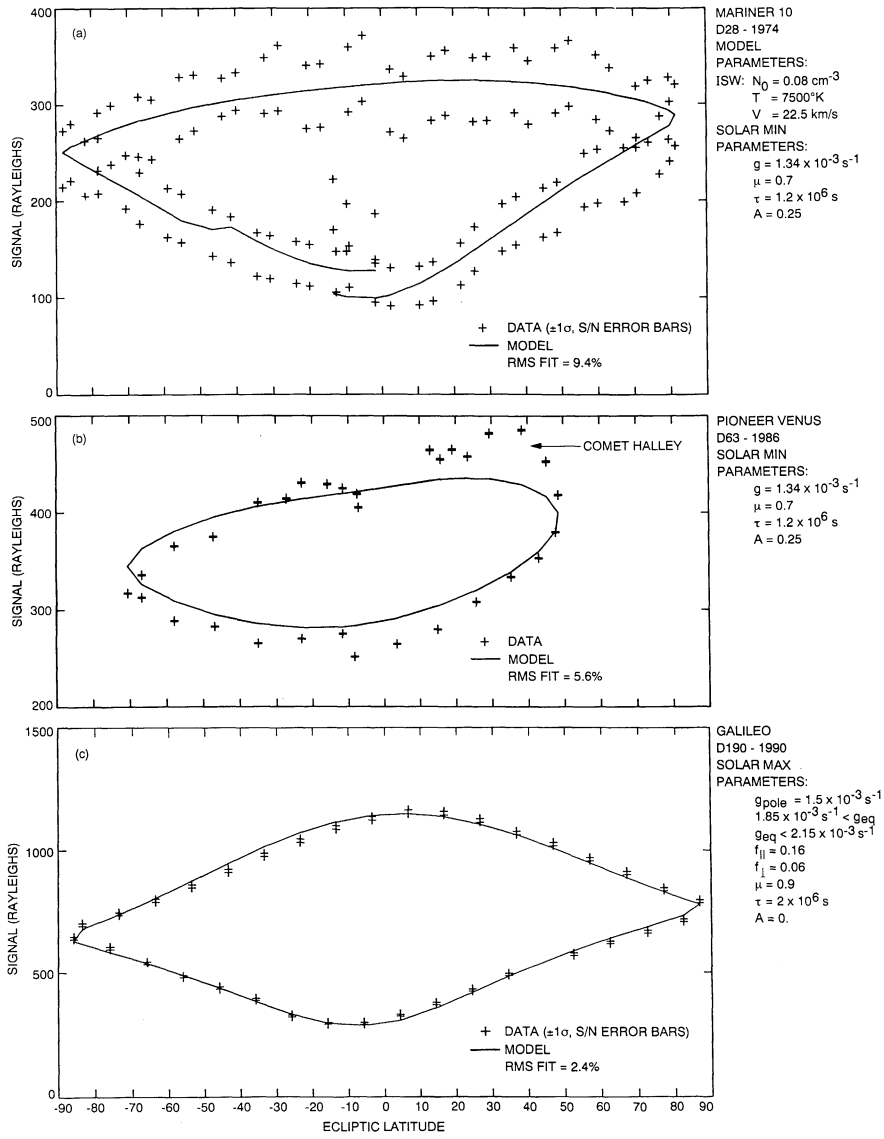

FIG. 14.—(*a*) The solar minimum model applied to *Mariner 10* IP Lyman-α data from 1974 DOY 28. (*b*) The solar minimum model applied to PVOUVS Lyman-α data from 1986 DOY 63. (*c*) The solar maximum model applied to *Galileo* EUVS data from 1990 DOY 190.

The analysis was repeated varying the phase between the solar flux and the observed emission. This is equivalent to imagining the Sun rotating with the Lyman-α flux at each solar longitude constant in time. The regression analysis showed a best fit with the longitudinal pattern of solar flux rotated 2 days (26°.7) past the sub-Earth point. The best fit of the four observational points on the 27 day pattern of the solar flux is shown in Figure 13. This technique of using the Sun as a searchlight to determine the location of the maximum indicates that there is a broad maximum centered at 312°. This compares with the model result of 303°. This difference of 9° is less than the discrete resolution of the solar flux data (13°.3) indicating that the searchlight technique produces a result that is consistent with the location of the source function as calculated in the model.

8. DISCUSSION

We can summarize the ability of the solar minimum and solar maximum models to fit the spacecraft IP Lyman-α observations with latitude. Figure 14 shows the *Mariner 10*, *PV*, and *Galileo* observations considered in this paper as a function of latitude. The models are applied at the extremes of the solar cycle and appear to explain the latitudinal variations well. The two models can be merged into a general model for application at any point in the solar cycle. The most important remaining task would be to include a time-dependent calculation of μ, the ratio of radiative pressure to gravitational force per atom, during the 1 year transit of the solar system by an interstellar hydrogen atom travelling at 22.5 km s^{-1}. The result that at solar maximum the g-value at the pole decreases by 25% between equator and pole implies substantial variation in μ with latitude along the incoming and outgoing asymptotes of the atom's trajectory at solar maximum.

The sensitivity of the model to solar parameters related to the solar wind (τ and A) and solar Lyman-α flux (g_{pole} and μ) are important considerations in the modeling process. The fitting process was tried with $g_{pole} = 1.4 \times 10^{-3}$ s^{-1}, 1.5×10^{-3} s^{-1}, and 1.6×10^{-3} s^{-1} with the other parameters identical to those in Figure 9. The smallest RMS error was obtained with $g_{pole} = 1.5 \times 10^{-3}$ s^{-1}. The sensitivity of the model to the other parameters is shown in Figures 15*a*, 15*b*, and 15*c* for τ, μ, and A, respectively. There is only a weak sensitivity of the model to each of these parameters. The value of τ is not well constrained. The value of τ is best determined by a direct measurement of the parallax shift (Ajello et al. 1987) or from solar wind flux measurements. Table 3 lists values of solar wind lifetimes for *IMP 8* data. The range of μ is $\mu = 0.9 \pm 0.2$ and $A = 0 \pm 0.2$.

Other considerations are quite important in ascertaining the correct parameters. For example, the downwind density is critically dependent on step size in the modeling interpolation procedure. A comparison of two different density models shows a 20% difference in the downwind direction. Figure 11 shows the Lyman-α emission source function in three nearly orthogonal directions using the modeling parameters given in Figure 9. A comparison of this model to another model developed by the University of Arizona (D. Hall, private communication) was made for the same three directions and for the same data set in Figure 9. The number density routine in this paper was developed by Thomas (1978) and obtains local densities by integrating over the distribution function at infinity. The University of Arizona code obtains densities by integrating over the distribution function at the space point.

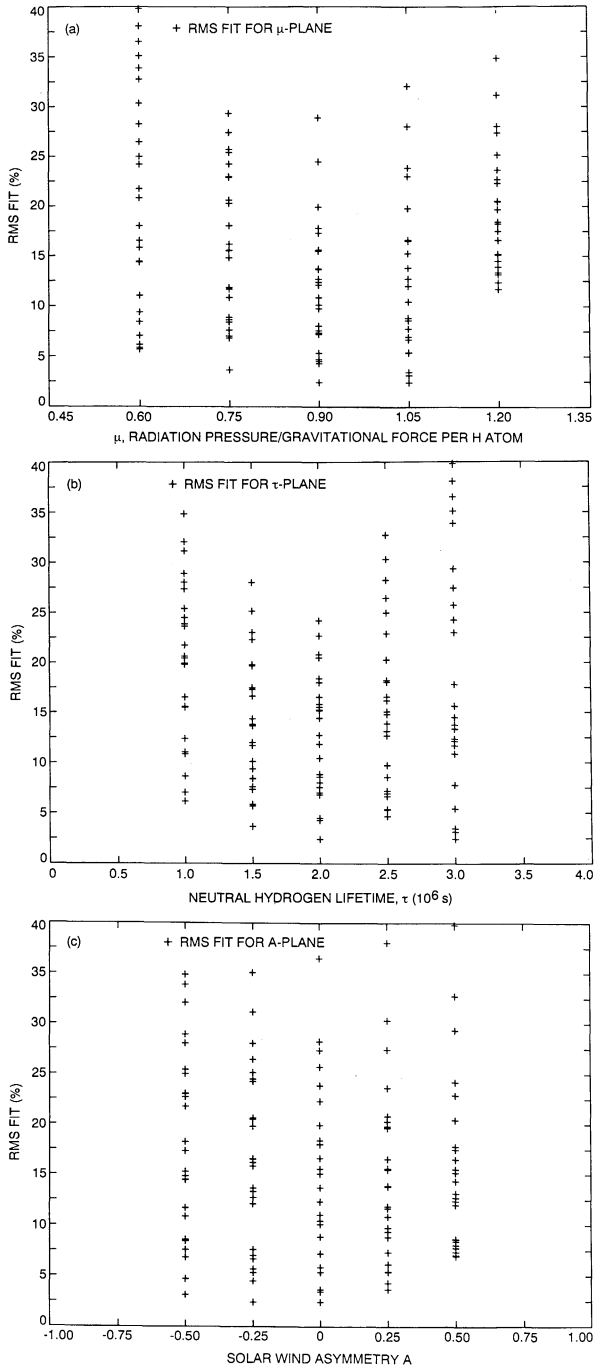

FIG. 15.—A sensitivity study was performed on the solar maximum model applied to 1990 DOY 190 *Galileo* EUVS data. A 5 × 5 × 5 grid of values of A, τ, and μ was used. (*a*) The RMS fit as a function of μ. (*b*) The RMS fit as a function of hydrogen lifetime τ. (*c*) The RMS fit as a function of the solar wind asymmetry factor A.

Upwind and sidewind intensity values agreed to within 7%. However 20% differences occurred downwind. These differences led to a slightly different value for the solar wind lifetime for the best fit. Solar wind lifetime is the most important parameter in establishing the downwind densities.

Future work with the *Galileo* data will concentrate on the residual differences between the data and the model in Figure 9. The remaining 1%–2% improvement in modeling uncer-

tainty is probably based on secondary effects not completely understood. A first effort was made to look into north/south asymmetries in the solar Lyman-α radiation field. Models at this point do not show any improvement in the fit for the particular data set DOY 190–200. The structure in Figure 9 indicates that the northern solar hemisphere may be ~5% brighter. However, UVS and EUVS observations in other spacecraft locations, e.g., downwind or upwind, may prove to be more sensitive to north and south asymmetries or to plage distributions with latitude. Additional models which account for the solar EUV latitude variation which are reflected in a latitude-dependent photoionization rate were tried. Initial results from these models do not lead to improved data fits, either. This effect will be discussed in the paper on *Galileo* EUV observations of He (58.4 nm). The EUV contrast factors for this model for the important EUV emissions in the Lyman-continuum have been measured by Reeves & Parkinson (1970). A rough approximation to the size of this effect is obtained by noting that photoionization is 25% of the total ionization loss rate at solar maximum. The latitude variation of solar EUV is also about 25%. Contrast factors for EUV emissions in the Lyman-continuum wavelength region are very similar to

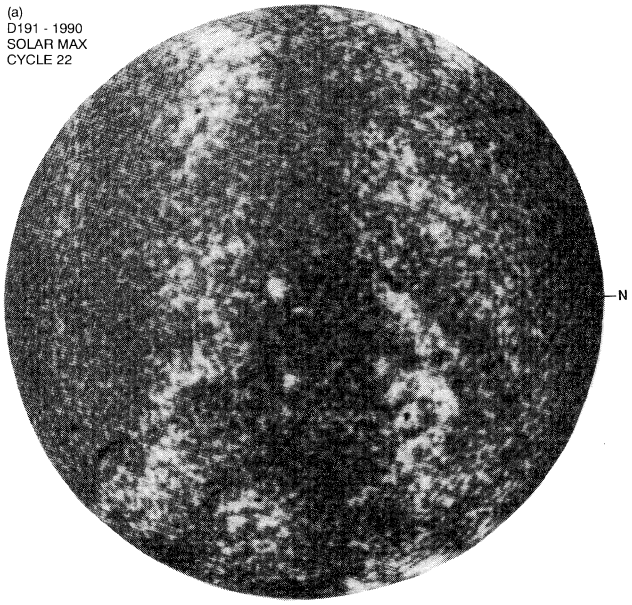

FIG. 16*a*

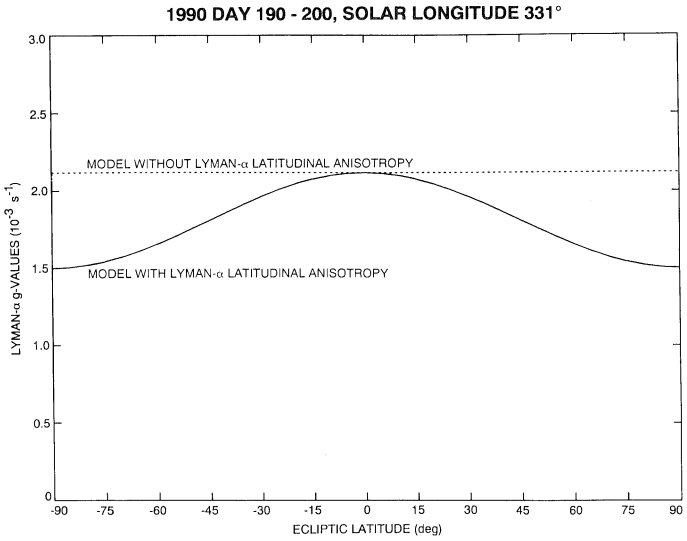

FIG. 16*b*

FIG. 16.—(*a*) A Ca II K image of the Sun on DOY 191 of 1990 showing the belts of activity near the solar equator. (*b*) The Lyman-α *g*-values in the solar maximum model as a function of latitude at a particular solar longitude (331°) during the period 1990 DOY 190–200. The enhancement in *g* near the equator is due to the two belts in (*a*). A constant *g*-value with latitude is also indicated illustrating the large difference the new solar maximum model makes near the poles.

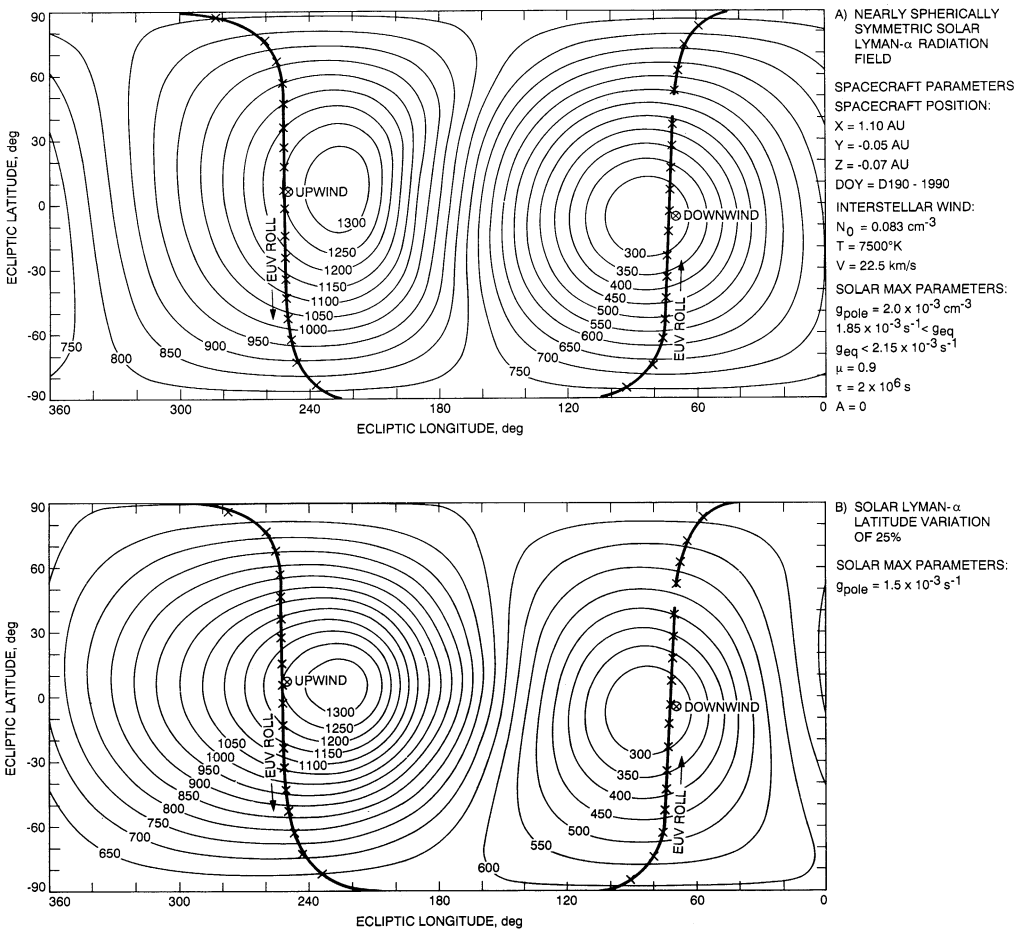

FIG. 17.—A predicted IP Lyman-α sky background isophote map for *Galileo* on DOY 190–1990 based on the model in Fig. 9 for the cases (*a*) nearly spherically symmetric solar Lyman-α and (*b*) solar latitude variation of solar Lyman-α of 25%. Model brightness values are in rayleighs. The spacecraft position is given in ecliptic *X*, *Y*, and *Z* coordinates. The EUVS line-of-sight direction on the celestial sphere for each of the 35 measurements in Fig. 9 is indicated by an X. A small region where no data collection occurs is indicated by a break in the solid curve through the observation points. The model in (*a*) assumes the latitude variation of solar Lyman-α is zero but uses the longitude variation of Table 2.

Lyman-α. Thus the maximum extent of the effect is a 6% decrease in the hydrogen atom photoionization rate from equator to pole.

We show the derived latitude variation for DOY 190 at ecliptic longitude 331° in Figure 16*b*. Figure 16*a* is a Ca II K image of the Sun showing the low-latitude bands of plage regions for DOY 191. The subsolar longitude of Earth was 336.8° ecliptic longitude. The image shows qualitative agreement between the modeled decrease of the *g*-value with latitude and the location of the plage regions. The models in Figures 9 and 10 can be used to give the extent of the latitude belt of plage regions from β_1 to β_2 as 0°–26°. The angular extent is calculated from the ratio of $f_\perp/f_\parallel$. The procedure is demonstrated in Cook et al. (1981), where it is shown that the important quantity is the average latitude of the plage belt. The model is only weakly dependent on the width. Thus we find the average latitude is 13° in rough agreement with the spectroheliogram of Figure 16*a*.

Finally in Figure 17 we show the model sky background isophote maps for the case (*a*) nearly spherically symmetric solar Lyman-α and for case (*b*) 25% solar Lyman-α latitude variation from the *Galileo* EUVS DOY 190 data at solar maximum. The parallax shift of ~20° for $\tau = 2.0 \times 10^6$ s and ~15° for $\tau = 1.5 \times 10^6$ s indicate that a sidewind spacecraft at 1–2 AU from the Sun with a UV spectrometer can be expected to observe a large parallax shift with a maximum value of near 90°. This measurement, in effect, is a sensitive measurement of ISW hydrogen lifetime. In addition, the solar Lyman-α latitude variation has an important effect on the shape of the isophotes. The larger the latitude variation of the solar Lyman-α the more the flattening of the isophotes. Note the north–south elongated isophotes near the upwind maximum in (*a*) are stretched and flattened in (*b*) due to the enhanced solar Lyman-α in the vicinity of the solar equator.

The research described in this paper was performed at the Laboratory for Atmospheric and Space Physics, University of Colorado and at the Jet Propulsion Laboratory, California Institute of Technology. This work was supported by the *Galileo* Project, the Space Physics Program Office, and the *Pioneer Venus* Guest Investigator Program. We have benefited from discussions with and programs and data provided by P. Bornman, J. Cook, R. Donnelly, L. Frank, D. Hall, A. Hundhausen, A. Lazarus, J. Lean, S. Martin, and D. Neidig.

REFERENCES

Ajello, J. M. 1978, ApJ, 222, 1068
———. 1990, J. Geophys. Res., 95, 14, 855
Ajello, J. M., Stewart, A. I., Thomas, G. E., & Graps, A. 1987, ApJ, 317, 964
Ajello, J. M., Witt, N., & Blum, P. W. 1979, A&A, 73, 260
Barth, C. A., Tobiska, W. K., Rottman, G. J., & White, O. R. 1990, J. Geophys. Res., 17, 571
Cook, J. W., Brueckner, G. E., & VanHoosier, M. E. 1980, J. Geophys. Res., 85, 2257
Cook, J. W., Meier, R. R., Brueckner, G. E., & VanHoosier, M. E. 1981, A&A, 97, 394
Hord, C. W., et al. 1991, Science, 253, 1548
Hord, C. W., et al. 1992, Space Sci. Rev., in press
Kumar, S., & Broadfoot, A. L. 1978, A&A, 69, L5
Lallement, R., & Stewart, A. I. 1990, A&A, 227, 600
Lean, J. 1987, J. Geophys. Res., 92, 839
Lean, J. L., & Skumanich, A. 1983, J. Geophys. Res., 88, 5751
Mihalov, J. D., Barnes, A., Hundhausen, A. J., & Smith, E. J. 1990, J. Geophys. Res., 95, 8231
Reeves, E. M., & Parkinson, W. H. 1970, ApJS, 21, 1
Rottman, G. J., & Barth, C. A., 1990, Eos, 71, 1480
Sheeley, N. R. 1967, ApJ, 147, 1106
Stewart, A. I. F. 1980, IEEE Trans. Geosci. Remote Sens., 18, 165
Thomas, G. E. 1978, Ann. Rev. Earth Planet. Sci., 6, 173
Thomas, G. E., & Anderson, D. E., Jr. 1976, Planet. Space Sci., 24, 303
Tobiska, W. K., & Barth, C. A. 1990, J. Geophys. Res., 95, 8243
Witt, N., Ajello, J. M., & Blum, P. W. 1979, A&A, 73, 272
———. 1981, A&A, 95, 80